Received: 6 May 2023 | Revised: 6 June 2023 | Accepted: 15 June 2023 | Published online: 16 June 2023

RESEARCH ARTICLE

Archives of Advanced Engineering Science
2024, Vol. 2(2) 71–78
DOI: 10.47852/bonviewAAES32021040

BON VIEW PUBLISHING

# Fabrication of N-Type Nanocrystalline Silicon Thin Film by Magnetron Sputtering and Antimony-Induced Crystallization

**Omid Shekoofa[1,*], Jian Wang[2] and Dejie Li[2]**

[1]*Department of Mechanical Engineering, Eastern Mediterranean University, Türkiye*

[2]*Electronic Engineering Department, Tsinghua University, China*

**Abstract:** The fabrication of n-type nanocrystalline silicon thin films using magnetron sputtering and crystallization by adding antimony and thermal treatment is presented in this article. Firstly, a short overview about thin-film deposition methods, along with the advantages and disadvantages of the magnetron sputtering, is provided. Then, the technique of adding metals for recrystallization of amorphous silicon is described, and the necessity of using antimony for obtaining n-type nanocrystalline silicon along with its characteristics is discussed. Next, the process of thin-film deposition using magnetron sputtering and the production of n-type nanocrystalline silicon on a quartz substrate, by antimony-induced crystallization, is explained. Subsequently, the characterization process and necessary measurements to confirm the crystallization of the nanocrystalline silicon layer and determine its crystalline properties are presented. For ease of electrical characterization, a simple n/p junction Schottky solar cell is fabricated using the produced nanocrystalline silicon layer on a p-type monocrystalline silicon wafer. In addition to nanocrystalline properties, the optical and electrical characteristics of this cell are also investigated. The measurements show that with the proposed method, a fine grains nanocrystalline silicon layer with an average grain size of 20 nm was formed in the <111> direction. J-V characteristic measurement shows the creation of a solar cell with conversion efficiency of 1.39%, open-circuit voltage of 265 mV, and current density of 16.32 mA/cm$^2$. These results confirm that antimony can be used in the process of crystallizing amorphous thin-film silicon obtained from magnetron sputtering and converting it into n-type nanocrystalline silicon.

**Keywords:** nanocrystalline, silicon, thin film, magnetron sputtering, antimony, thermal annealing

## 1. Introduction

Thin-film polysilicon is a widely used material in the electronics industry, which has been used for many years in the fabrication of transistors, Thin-Film Transistor (TFT) displays, solar cells, optoelectronic devices, and more recently in the production of microelectromechanical) components and non-volatile Blu-ray memories (Abo Ghazala et al., 2020; Fortunato, 1997; Haschke et al., 2014; Her et al., 2009; Sharma et al., 2014). In most cases, the polysilicon fabrication process involves chemical vapor deposition (CVD) techniques, such as metalorganic chemical vapor deposition and plasma-enhanced chemical vapor deposition, which are extensively employed for this purpose (Prayogi et al., 2023). Despite the advantages of high precision in film deposition and excellent quality of grown polysilicon using these methods, it should be acknowledged that these methods have inherent and significant challenges such as high fabrication costs, complexity of required equipment, the need for high-temperature deposition processes, use of toxic and explosive gases, and limitations in film deposition dimensions (Safi, 2000; Tüzün et al., 2010).

According to Figure 1 (Babu & Moorthy, 2015; Ennaoui, 2012), one of the alternative solutions is to use magnetron sputtering, which is considered as a type of physical thin film deposition and has developed significantly in the recent years due to its numerous advantages. These advantages include the low temperature deposition, high efficiency in the use of raw materials, scalability to large dimensions, and higher environmental compatibility due to the absence of chemical, toxic, and explosive materials within the sputtering process. Additionally, the working conditions and process control are easier, and the required equipment is cheaper and simpler due to the use of solid-state materials for film deposition (such as silicon and metal targets) (Fujimura et al., 2015).

However, the deposition of materials using the magnetron sputtering has a major drawback, which is the non-crystalline and amorphous nature of the final product of this process. The thin film obtained from silicon sputtering has abundant dangling bonds between silicon atoms, which can act as recombination centers for the majority charge carriers and fundamentally affect the electrical properties of the film. One approach to neutralize these dangling bonds is to use hydrogen which can combine with incomplete

*Corresponding author: Omid Shekoofa, Department of Mechanical Engineering, Eastern Mediterranean University, Türkiye. Email: omid.shekoofa@emu.edu.tr

© The Author(s) 2023. Published by BON VIEW PUBLISHING PTE. LTD. This is an open access article under the CC BY License (https://creativecommons.org/licenses/by/4.0/).

**Figure 1**
**Different thin-film deposition methods**

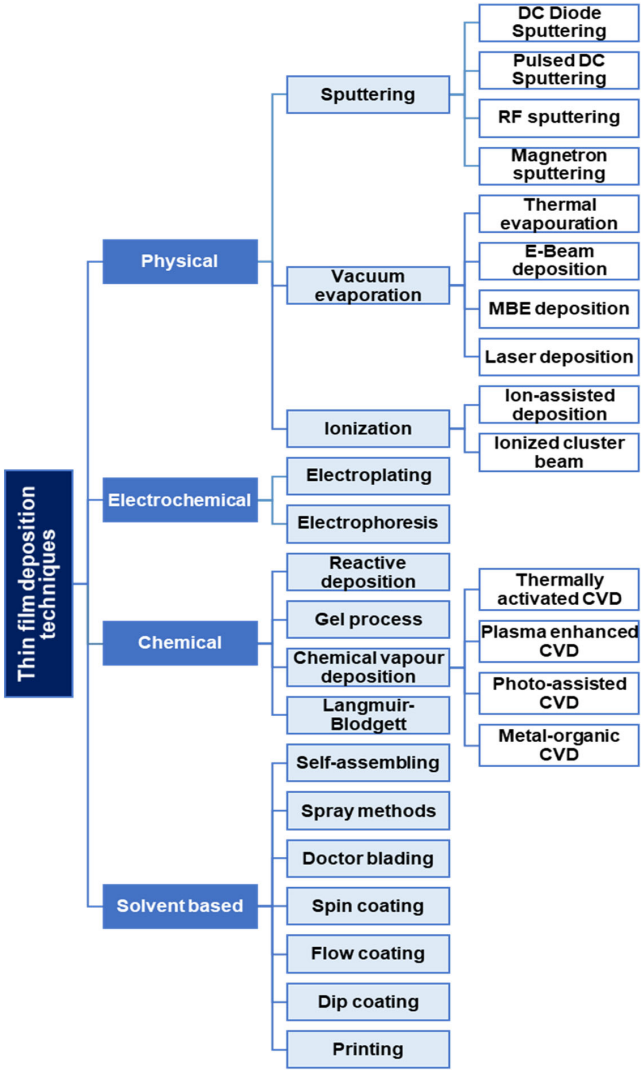


bonds and neutralize them in the deposition process. The thin-film silicon prepared by this method is denoted as a: Si-H. This structure is still in an amorphous state and for many applications it requires another step to be crystallized. Furthermore, the use of hydrogen gas itself is hazardous and problematic, as it is flammable and explosive, and deposition systems involving hydrogen flow are more complex and must have sufficient safety measures (Hamasha et al., 2016).

A fundamental solution to address this issue is to apply a heat treatment process to the thin silicon layers, which will result in the silicon recrystallization (Baskar, 2019; Wilken et al., 2022). However, this solution faces a major problem, which is that the recrystallization of silicon begins at temperatures above 900°C, and complete crystallization of the amorphous film requires higher temperatures and longer heat treatment times. These conditions result in complexity, increased costs, and impracticality of this method.

One approach to overcome this challenge is to add metal atoms to the thin silicon layer prepared by the sputtering method and then perform a thermal annealing process on it. In this process which is called metal induced crystallization, metal atoms contribute to the creation of polycrystalline silicon, by neutralizing free bonds and reducing the temperature required to initiate the crystallization process, resulting in lower energy and temperature needed for the creation of polycrystalline layer from amorphous silicon (Maity, 2022). This allows the use of cheaper substrate materials that can withstand lower temperatures as a silicon device substrate. However, the structure of the resulting polycrystalline layer can have varying quality and specifications depending on various factors of magnetron sputtering, such as temperature, pressure, thickness and sequence of layers, temperature profile, purity of the metal material, and level of impurities (Becker, 2013; Gall, 2009).

The mechanism of silicon crystallization by adding metals has been extensively studied, and this process has been widely used to prepare polycrystalline silicon layers with p-type doping using atoms such as aluminum (Maity, 2019; Shekoofa, 2017), copper (Shekoofa et al., 2020), tin (Neimash, 2014), and nickel (Schmidt et al., 2009). However, the use of this method for n-type doping requires further investigation and optimization, due to the special properties of materials that can create n-type doping. Therefore, the idea of this research is to attempt to create n-type thin-film silicon by sputtering and crystallization with the help of adding a suitable metal.

After this introduction, the organization of different sections of the paper is as follows. The materials and method of the research are introduced in Section 2. It includes the details of the deposition method, the specifications of the used equipment, and the list of applied characterization tests. In Section 3, the results of each characterization techniques are presented and discussed one by one. Finally, the last section is dedicated to the conclusion and the proposed future works.

## 2. Materials and Methods

To create n-type polysilicon, the best material that can be added to amorphous silicon is phosphorus, a group 5 element, which is commonly used in CVD deposition methods to create n-type silicon. However, phosphorus cannot be used in magnetron sputtering because the material that is co-deposited with silicon in sputtering must be solid and stable, and capable of transforming into targets used in sputtering machines. Additionally, phosphorus is toxic and harmful to human health.

The substitute element for phosphorus must have an ionization energy level close to the conduction level of silicon in order to function as an n-type dopant. By referring to the ionization energy diagrams of various impurities in combination with silicon (Figure 2 (Ionization Energy/Dopant Energy Levels of Impurities in Crystalline Silicon (Olesinski & Abbaschian, 1985))), it can be seen that elements such as phosphorus, lithium, arsenide, and bismuth are not suitable for this purpose due to various reasons such as instability, toxicity, and high cost.

The only suitable element for this purpose is antimony, which is capable of transforming into targets, is non-toxic, and has stability in the laboratory and sputtering process conditions (Figure 2 left (Ionization Energy/Dopant Energy Levels of Impurities in Crystalline Silicon)). However, the main advantage of antimony in the crystallization process is demonstrated by its binary compound with silicon. Adding antimony to silicon reduces the crystallization threshold temperature of silicon from approximately 900°C down to about 660°C (Figure 2 right (Olesinski & Abbaschian, 1985)).

At the same time, a kind of n-doping also occurs in this process, due to the ionization of a percentage of silicon atoms and the substitution of antimony atoms with them (Carlsson et al., 1997; Ohmura, 2003). In this process, the crystallization of silicon follows the mechanism of metal layer exchange, where during a thermal annealing process, an amorphous layer of silicon in

**Figure 2**
**Left: The energy ionization diagram of various impurities in silicon. Right: Si-Sb binary phase diagram**

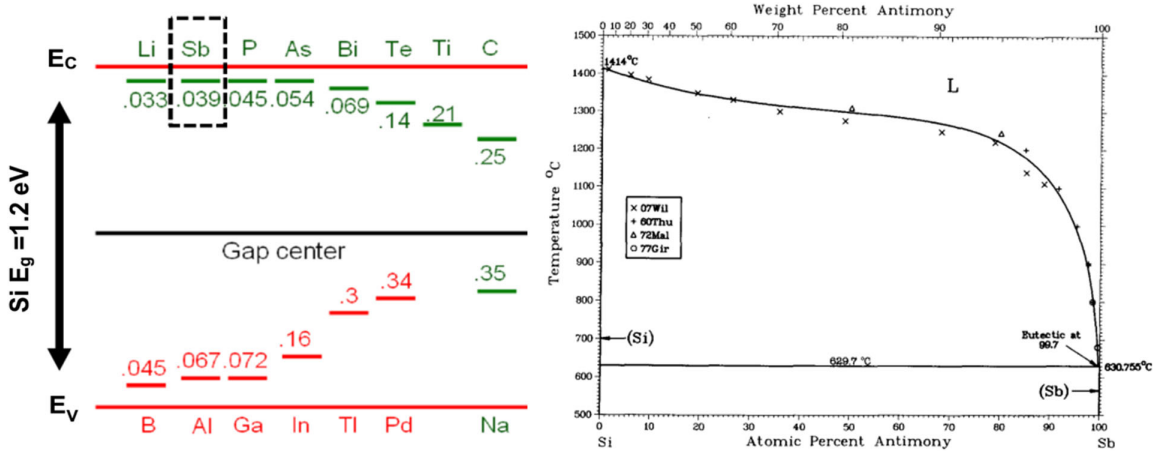


contact with a thin layer of certain metals can acquire a crystalline structure while displacing the layers order. The occurrence of this layer exchange has been extensively studied in various references (Kuraseko et al., 2009; Nast & Wenham, 2000). In this study, the Si/Sb/Substrate structure (with antimony layer prior to the silicon layer) was used to create a thin layer of nanocrystalline silicon after the heat treatment and layer exchange between the metal and silicon layers.

## 2.1. Specifications of deposition process

All the deposition processes in this experiment were performed using a MSP3200P magnetron sputtering machine. Two types of substrates and four types of sputtering targets were used in these experiments. The specifications of the substrates and targets used in this process are presented in Table 1.

The specifications of the deposition process are presented in Table 2. The preparation of the magnetron sputtering system for the thin-film deposition process is done as follows: the chamber evacuation starts and continues until the pressure reaches 0.0001 Pa after placing the targets in designated positions. The heater of the sample holder is turned on at the beginning of the chamber evacuation process. The temperature of the substrate gradually increases with the start of the chamber evacuation and reaches 140°C. If the temperature is suddenly increased at the beginning, the final temperature may exceed the predetermined value by several degrees. If the substrate heating starts with the sputtering process, the actual vacuum level will be worse than the predetermined vacuum level indicated in Table 2 (due to the lack of sufficient time for the evacuation of evaporated impurities), and it will negatively affect the quality of the deposited micro-silicon (Ruan, 2019).

After the base vacuum pressure was less than 1 mPa and the sample holding temperature (substrate temperature) reached 140°C, argon gas was introduced into the chamber with a flow rate of 40 sccm until the vacuum pressure increased to 1.2 Pa at the threshold of the deposition process and the main part of the layering process can begin.

Figure 3 illustrates the steps of the deposition process to create a n/p solar cell by n-type thin-film nanocrystalline silicon. Initially, a 100 nm layer of antimony is deposited, followed immediately by a 100 nm layer of n-type silicon under the conditions listed in Table 2, on substrates made of p-type monocrystalline silicon wafers and on quartz pieces (for characterization purpose). After removing the deposited thin-film samples from the sputtering machine and cutting them into smaller pieces, multiple samples were prepared for thermal annealing operations.

**Table 1**
**The specifications of the substrates and targets used in this study**

| Material | Dimension/ Diameter (mm) | Thickness (mm) | Purity (%) |
|---|---|---|---|
| Antimony target | 80 | 5 | 99.99 |
| n-Type silicon target | 80 | 3 | 99.99999 |
| Silver target | 80 | 5 | 99.99 |
| Aluminum target | 80 | 5 | 99.99 |
| p-type monocrystalline Si wafer (CZ <100>), resistivity of 1–10 Ω.cm | 50.8 | 0.300 | 99.99999 |
| Quartz glass substrate | 10 × 10 | 1 | – |

**Table 2**
**Sputtering parameters for the thin-film deposition in this study**

| Deposition parameters | Sb | n-Si | Dimension |
|---|---|---|---|
| Base pressure | $<10^{-3}$ | $<10^{-3}$ | [Pa] |
| Sputtering pressure | 1.2 | 1.2 | [Pa] |
| Sputtering power | 60 | 250 | [W] |
| Duration | 140 | 310 | [s] |
| Deposition rate | 0.7 | 0.32 | [nm/s] |
| Thickness | 100 | 100 | [nm] |
| Ar flow rate | 40 | 40 | [sccm] |
| Substrates temperature | 140 | 140 | [°C] |

## 2.2. Thermal annealing process

The deposited thin-film samples on the different substrates, i.e., wafer and quartz glass, were subjected to heat treatment at different temperatures ranging from 500°C to 900°C, through a three-phase process as displayed in Figure 3.

**Figure 3**
**The three different regions of (a), (b), and (c) in a typical applied heat treatment profile for the maximum temperature of 500°C**

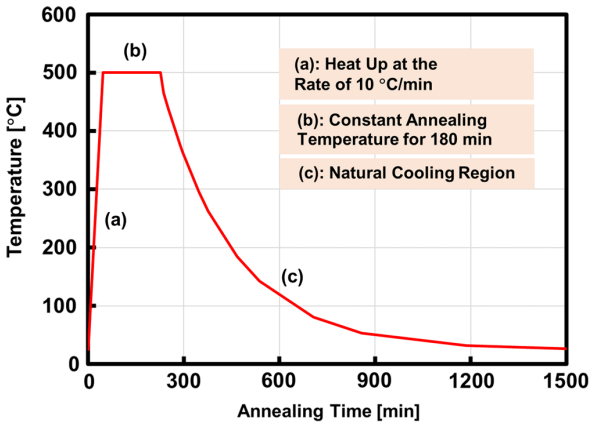


- Phase (a): increasing the temperature by 10° per minute from room temperature to the final temperature,
- Phase (b): maintaining the temperature for 180 min,
- Phase (c): natural cooling process.

During this process, various samples of n-type nanocrystalline silicon with different characteristics were obtained due to the occurrence of the so-called silicon and antimony layers displacement process.

## 2.3. Electrodes fabrication

In the final step of the sample fabrication process, four silver electrode pads, with dimensions of 1 mm × 1 mm and a thickness of 250 nm, were deposited on the four corners of the sample to perform electrical characterization tests on samples with quartz substrate. For the samples deposited on silicon wafer substrate, firstly a 250 nm thick layer of aluminum was deposited on the entire back of the sample, and then using an appropriate pattern mask, metal electrodes with the same thickness made of silver were deposited on the surface of the thin-film layer, creating a basic n/p junction Schottky solar cell (as shown in the step 5 of Figure 4).

The reason for using silver for the top electrodes compared to aluminum is that since the nanocrystalline layer is n-type, the aluminum atoms can neutralize the effects of antimony impurities, converting the regions under and around the electrodes to intrinsic semiconductors, which increases the internal resistance of the layer and the series resistance of the solar cell. On the other hand, silver electrodes do not have this effect and can maintain the desired characteristics of the nanocrystalline n-type layer.

## 2.4. Characterization tests and specifications of the measuring equipment

After depositing the thin-film layer and fabricating the necessary electrodes, the next step is to perform different tests and measurements to verify the formation of crystalized silicon thin film, determine the crystal structure and quality, and its electrical characteristics. Raman and X-Ray Diffraction (XRD) tests were used to determine the crystalline properties of the thin-film material. The optical and electron microscopes were used to examine the morphological properties of the samples, and J-V curves were measured to determine the electrical characteristics in dark and illuminated conditions. Raman spectrum measurements were performed using a LabRam HR spectrometer manufactured by Horiba, equipped with a laser beam with a wavelength of 532 nm. XRD tests were conducted using a SmartLab system manufactured by Rigaku equipped with a Bruker D8 diffractometer and a CuKα source with a wavelength of $\lambda\alpha 1 = 1.5406$ Å. An Olympus BH3-WHP6 optical microscope and a JSM-7001F electron microscope manufactured by JEOL were used for the examination of the morphological properties of the nanocrystalline layer. Finally, J-V characteristic measurements were performed using a Keithley-2400 source meter and a solar simulator system model XES-70S in dark and illuminated (AM1.5G standard irradiance) conditions, respectively.

## 3. Results and Discussion

In the first step of the characterization process, Raman spectra of different samples were measured and the amount of corresponding

**Figure 4**
**Different steps of the solar cell fabrication process by n-type thin-film nanocrystalline silicon**

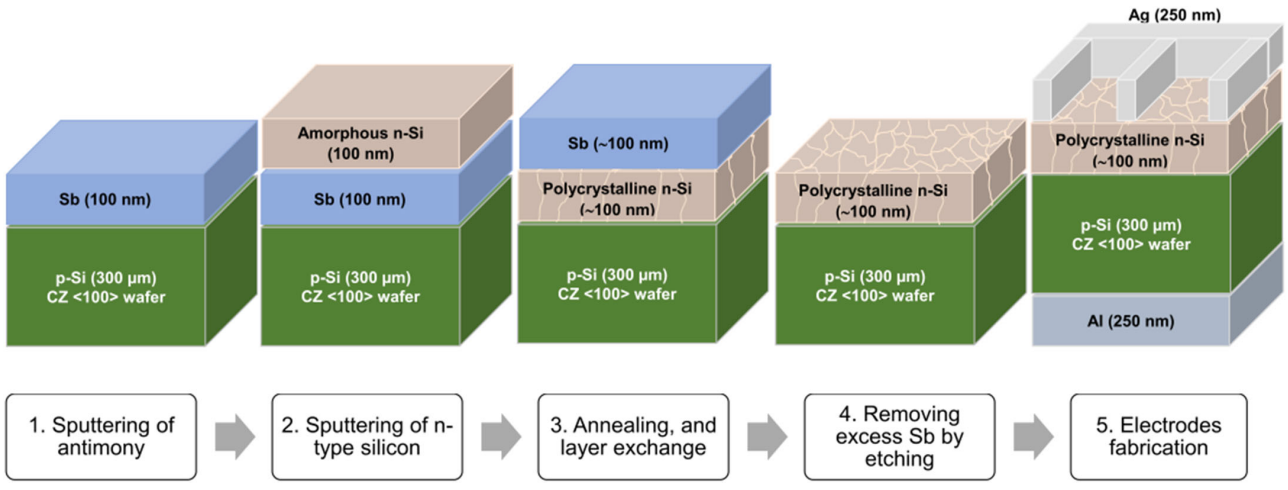

**Figure 5**
**The state of Raman spectrum peak shift in the thin-film sample prepared at different temperatures and their crystallization percentage per temperature (inset diagram)**

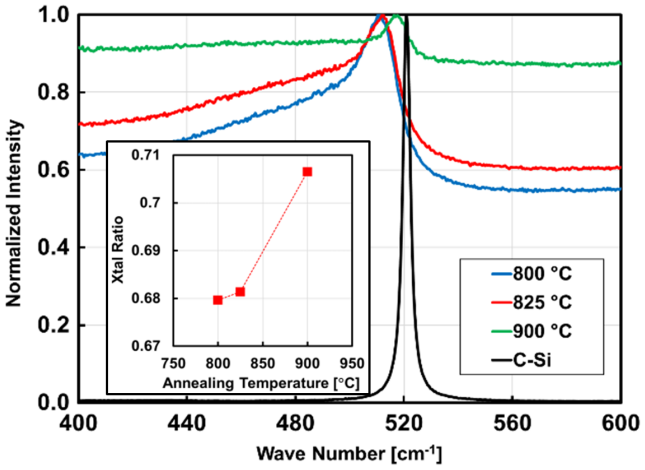


Raman peak shifts was examined to confirm the formation of the nanocrystalline layer and determine the crystallization ratio at different annealing temperatures. In Figure 5, which shows the normalized Raman spectra for three nanocrystalline samples prepared at three different temperatures, the Raman peak is observed at around 825 $cm^{-1}$ and shifts to 517 $cm^{-1}$ with increasing temperature up to 900°C, but does not reach the wavenumber of 520 $cm^{-1}$, which corresponds to the peak of the reference monocrystalline silicon sample. The crystallization percentage of the thin film was calculated by using equation (1), where $I_c$, $I_m$, $I_a$ represent the intensities of the crystalline, nanocrystalline, and amorphous components, respectively (Chen et al., 2014).

$$R_x = (I_c + I_m)/(I_c + I_m + 0.85 \times I_a) \quad (1)$$

The small diagram in Figure 5 indicates the relatively low percentage of crystallization of the n-type silicon nanocrystalline layer prepared in this process, which is about 68% at temperatures of 800–825°C and changes only slightly to 71% as the temperature increases to 900°C.

In the next step, XRD spectra of various samples were evaluated to determine the crystal structure and orientation of the prepared nanocrystalline thin films, by examining the location and intensity of the peaks related to the silicon crystal directions. According to the results which are shown in Figure 6, a very small peak at the angle of 28.5° is observable even at a low temperature of 500°C, but the distinct peak corresponding to Si <111> direction can only be observed at temperatures higher than 600°C. A clear peak is observed at 825°C, and this peak becomes much stronger at 950°C. By studying the corresponding peak to <111> orientation at the angle of 28.5° and it is determined that the grain size of the crystals at this temperature is approximately 20 nm using the Bragg's law. However, at 950°C, peaks corresponding to the <220> and <311> directions are also observable, but due to their broadness and low height, the crystal grain size related to these peaks must be smaller. The presence of these peaks confirms the deterioration of the quality of the nanocrystalline layer prepared at temperatures higher than 900°C using this method, which makes it unsuitable for many applications.

**Figure 6**
**The occurrence of the peak related to Si <111> and its strengthening with increasing temperature**

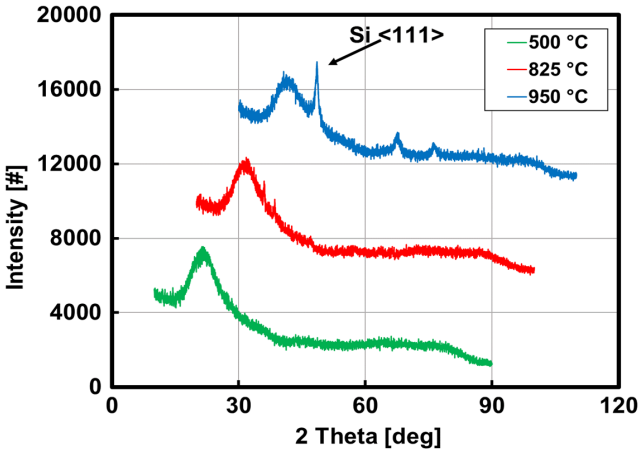


(note: the red and blue curves have been shifted along the horizontal and vertical axes for better visibility)

**Figure 7**
**Crystal structure formation nuclei (yellow arrows) and crystallized regions (yellow circles) of silicon thin film on quaternary substrate**

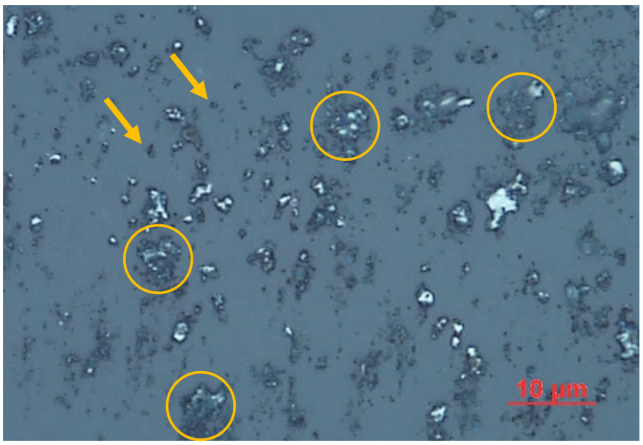


After confirming the formation of the crystalline structure in the produced silicon thin film, the morphology of the samples deposited on the quartz substrate was examined by optical microscopy, as shown in Figure 7. According to this figure, a significant portion of the surface of the sample prepared at 850°C is still uncrystallized, and the silicon-antimony binary compound remains in an amorphous form. Although multiple nucleation sites for crystal formation can be seen in this image (such as the points marked with yellow arrows), only a few of these centers have grown enough to create a few-micron-sized structure in the form of clusters of crystalline silicon (yellow circles). Due to the relatively large distance and sparsity of these clusters, a homogeneous layer or at least a continuous layer has not formed.

In the next step, the grown thin-film layers on the silicon wafer substate were analyzed by SEM imaging. As shown in Figure 8, dark areas (enclosed by yellow curves) were observed among the relatively homogeneous and bright surface of the sample after

**Figure 8**
**Crystallized (enclosed by yellow curve) and non-crystallized regions after heat treatment, compared to the structure of the sample before heat treatment (red box)**

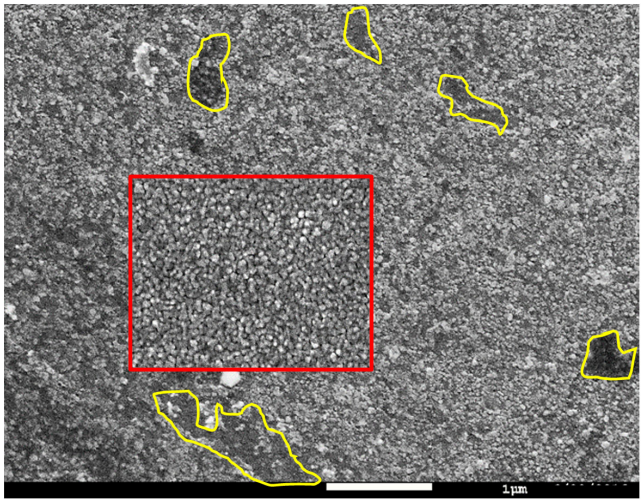


**Figure 9**
**J-V characteristics curve in the dark and under irradiation, for the solar cell fabricated at 850°C on the CZ <100> p-type silicon wafer**

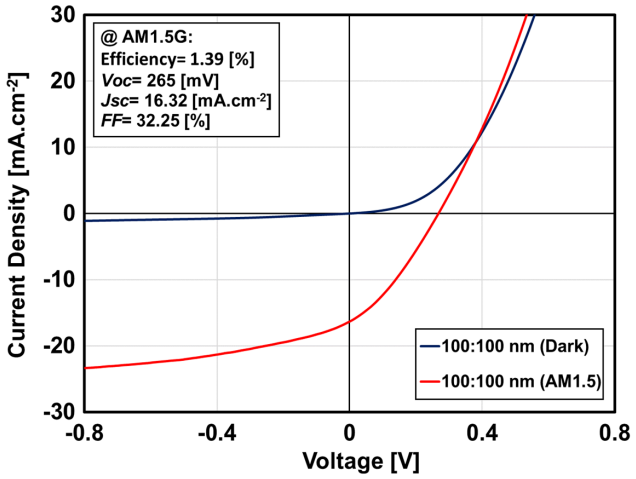


annealing the sample at 850°C. In addition to the formation of such dark regions, which are the evidence of the crystallization of the amorphous silicon, there is significant difference in surface texture between the unannealed sample (red box) and the heat-treated sample which clearly indicates the effects of temperature on the silicon thin film under study. In fact, the primary amorphous structure has been transformed into a relatively uniform crystallized layer with crystal sizes ranging from tens to hundreds of nanometers.

Following the crystal properties, the electrical characteristics of the n-thin film Si/p-mono Si substrate were also investigated in this study. The J-V characteristic curve of the silicon thin film processed after thermal treatment at 850°C on p-type monocrystalline silicon wafers was measured under both dark and standard AM1.5G illuminated conditions, resulting in a curve shown in Figure 9.

**Figure 10**
**Examples of the low adhesion issue of the fabricated thin films on different substrates after thermal annealing at 850°C**

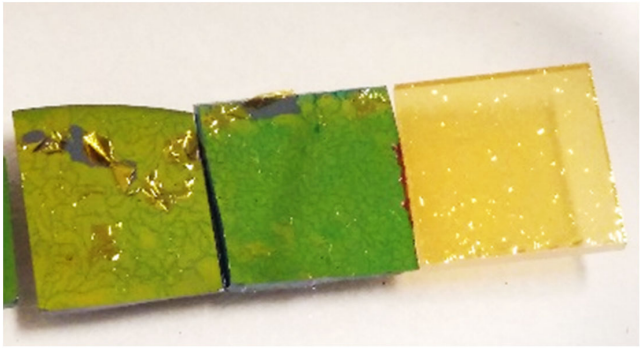

The main characteristics of this simple solar cell were an open-circuit voltage of 265 mV, a short-circuit current of 16.32 mA/cm$^2$, and an overall efficiency of 1.3%. Despite its low efficiency, the photovoltaic behavior of this sample indicates that the thin silicon layer prepared has been reasonably crystallized and doped with the n-type impurity, both of which are due to the influence of adding antimony atoms to the amorphous silicon.

Further analysis of the reverse-bias region of the J-V characteristic curve reveals that the reverse saturation current of the p-n junction created (the magnitude of the current at negative bias voltages under dark condition) is high, while the parallel resistance of the solar cell (the flatness of the red curve in reverse bias) is low. Both factors, which are affected by the low quality and lack of continuity of the produced nanocrystalline silicon layer, reduce the efficiency of this solar cell. In the forward-bias region, it is observed that the series resistance (the slope of the red line at zero current) is very high, which may be due to the presence of numerous uncontrolled impurities in the prepared nanocrystalline sample, the small size of crystalline grains, the oxidation of the surface of the nanocrystalline film during the cooling process after thermal treatment, and the lack of appropriate electrical conduction of the metallic electrodes on the film surface. These issues have also resulted in an overall reduction in the fill factor of the solar cell which is limited to almost 32%.

In the last part of the characterization process, the visual inspection of some of the fabricated samples was carried out which showed a major issue with the quality of the n-type poly-Si thin-film created by antimony-induced crystallization. Figure 10 shows three samples which exhibit the peeling of the poly-Si films after thermal annealing at 850°C. This is resulted from the instability and low adhesion of the created poly-Si layer to the C-Si or glass substrates after heat treatment, which may happen even after annealing at relatively low temperature of 500°C. Such problem has been reported in some other research too (Wang et al., 2008). The problem is getting severer especially at the higher temperatures when more excess Sb content, transferred to the top of the poly-Si after annealing, and it must be removed by chemical etching before electrode contacts fabrication. This low adhesion and bonding force can lead to form a poor mechanical interface between the created n-type layer and p-type substrate and reduce the performance of the p-n junction in terms of its photovoltaic energy conversion. It should be noted such condition has not been reported for aluminum- and copper-induced crystallization of amorphous silicon.

## 4. Conclusion

In this study, a simple and environmentally friendly method (without using any toxic or hazardous chemical substances) was investigated for the fabrication of n-type nanocrystalline silicon thin films. We used the magnetron sputtering technique with the addition of antimony metal, followed by thermal treatment for this purpose. Different characterizations were carried out on two sets of samples fabricated on monocrystalline Si wafer and quartz glass substrates. The measurements confirmed the formation of a nanocrystalline silicon layer mainly with a crystal orientation of <111>, the average crystal grain size of about 20 nm, and lengths of the crystallized regions ranging from a few tens to a few hundred nanometers. A simple solar cell composed of this thin film of nanocrystalline on a p-type silicon wafer was created, and its electrical characteristics were measured. According to the measured J-V curves under dark and illuminated conditions, the fabricated solar cell showed a significant photovoltaic property, with a short-circuit current density of more than 16 mA/cm$^2$ under AM1.5G irradiation. However, due to some process flaws such as impurities in the antimony target, the residual atoms inside the sputtering chamber, and oxidation of the nanocrystalline layer during and after the thermal treatment process, the quality of the obtained thin-film layer was not satisfactory, and its improvement requires further research.

## Ethical Statement

This study does not contain any studies with human or animal subjects performed by any of the authors.

## Conflicts of Interest

Omid Shekoofa is the Editorial Board Member for *Archives of Advanced Engineering Science*, and was not involved in the editorial review or the decision to publish this article. The authors declare that they have no conflicts of interest to this work.

## Data Availability Statement

Data available on request from the corresponding author upon reasonable request.

## References


Abo Ghazala, M. S., Othman, H. A., Sharaf El-Deen, L. M., Nawwar, M. A., & Kashyout, A. E. B. (2020). Fabrication of nanocrystalline silicon thin films utilized for optoelectronic devices prepared by thermal vacuum evaporation. *ACS Omega*, *5*(42), 27633–27644. http://doi.org/10.1021/acsomega.0c04206.

Babu, S., & Moorthy, K. (2015). *Thin film structures in energy applications*. USA: Springer Cham. http://doi.org/10.1007/978-3-319-14774-1.

Baskar, S., Azam, A. B., Akshay, S., Thomas, N. S., Devesh, M., Hariprasath, B., & Nalini, R. P. (2019). Effect of thermal annealing on the structural, optical and microstructural properties of a-SiC thin films. *Advances in Materials and Processing Technologies*, *5*(3), 438–444. http://doi.org/10.1080/2374068X.2019.1622298.

Becker, C., Amkreutz, D., Sontheimer, T., Preidel, V., Lockau, D., Haschke, J., . . . , & Rech, B. (2013). Polycrystalline silicon thin-film solar cells: Status and perspectives. *Solar Energy Materials and Solar Cells*, *119*, 112–123. http://doi.org/10.1016/j.solmat.2013.05.043.

Carlsson, J. R. A., Sundgren, J. E., Madsen, L. D., Li, X. H., & Hentzell, H. T. G. (1997). Thermal stability and crystallization of amorphous Si1-xBx, Si1-xPx and Si1-xSbx alloy thin films. *Thin Solid Films*, *300*, 51–58.

Chen, I., Lin, P. Y., Li, T. T., & Chang, J. Y. (2014). Kinetic study of the thermal crystallization behavior of hydrogenated amorphous silicon prepared by ECRCVD. *ECS Journal of Solid State Science and Technology*, *3*(5), N75–N82. http://doi.org/10.1149/2.018405jss.

Ennaoui, A. (2012). PVSEC-Part III, Fundamental and application of Photovoltaic solar cells and system, Courses on photovoltaic for Moroccan academic staff; 23–27 April 2022, ENIM/Rabat, Helmholtz-Zentrum Berlin für Materialien und Energie.

Fortunato, G. (1997). Polycrystalline silicon thin-film transistors: A continuous evolving technology. *Thin Solid Films*, *296*(1), 82–90. https://doi.org/10.1016/S0040-6090(96)09378-9.

Fujimura, S., Someya, T., Yoshiba, S., Tsukamoto, T., Kamisako, K., & Suda, Y. (2015). Low-temperature fabrication technologies of Si solar cell by sputter epitaxy method. *Japanese Journal of Applied Physics*, *54*(8S1), 08KD01. http://doi.org/10.7567/JJAP.54.08KD01.

Gall, S., Becker, C., Conrad, E., Dogan, P., Fenske, F., Gorka, B., . . . , & Rech, B. (2009). Polycrystalline silicon thin-film solar cells on glass. *Solar Energy Materials & Solar Cells*, *93*, 1004–1008. http://doi.org/10.1016/j.solmat.2008.11.029.

Hamasha, K., Hamasha, E., Masadeh, G., Shariah, A., & Hamasha, M. M. (2016). Aluminum-induced crystallization of hydrogenated amorphous silicon thin films with assistance of electric field for solar photovoltaic applications. *Journal of Display Technology*, *12*(1), 82–88. http://doi.org/10.1109/JDT.2015.2457892.

Haschke, J., Amkreutz, D., Korte, L., Ruske, F., & Rech, B. (2014). Towards wafer quality crystalline silicon thin-film solar cells on glass. *Solar Energy Materials and Solar Cells*, *128*, 190–197. http://doi.org/10.1016/j.solmat.2014.04.035.

Her, Y. C., Chen, J. H., Tsai, M. H., & Tu, W. T. (2009). Nickel-induced crystallization of amorphous Ge film for blue-ray recording under thermal annealing and pulsed laser irradiation. *Journal of Applied Physics*, *106*(2), 1–6. http://doi.org/10.1063/1.3183956.

Ionization energy/dopant energy levels of impurities in Crystalline Silicon. Retrieved from: http://www.globalsino.com/EM/page2777.html

Kuraseko, H., Orita, N., Koaizawa, H., & Kondo, M. (2009). Inverted aluminum-induced layer exchange method for thin film polycrystalline silicon solar cells on insulating substrates. *Applied Physics Express*, *2*(1), 0155011–0155013. http://doi.org/10.1143/APEX.2.015501.

Maity, G., Singhal, R., Dubey, S., Ojha, S., Kulriya, P. K., Dhar, S., . . . , & Patel, S. P. (2019). Aluminum induced crystallization of amorphous Si: Thermal annealing and ion irradiation process. *Journal of Non-Crystalline Solids*, *523*, 119628, http://doi.org/10.1016/j.jnoncrysol.2019.119628.

Maity, G., Dubey, S., Meher, T., Dhar, S., Kanjilal, D., Som, T., & Patel, S. P. (2022). Perspectives on metal induced crystallization of a-Si and a-Ge thin films. *RSC Advances*, *12*(52), 33899–33921. http://doi.org/10.1039/D2RA06096E.

Nast, O., & Wenham, S. R. (2000). Elucidation of the layer exchange mechanism in the formation of polycrystalline silicon by aluminum-induced crystallization. *Journal of Applied Physics*, *88*(1), 124–132. http://doi.org/10.1063/1.373632.

Neimash, V. B., Goushcha, A. O., Shepeliavyi, P. E., Yukhymchuk, V. O., Dan'ko, V. A., Melnyk, V. V., & Kuzmich, A. G. (2014). Mechanism of Tin-induced crystallization in amorphous silicon. *Ukrainian Journal of Physics*, *59*(12), 1168–1176. http://doi.org/10.15407/ujpe59.12.1168.

Ohmura, Y., Takahashi, M., Suzuki, M., Emura, A., Sakamoto, N., Meguro, T., & Yamamoto, Y. (2003). N-type (P, Sb) and p-type (B) doping of hydrogenated amorphous Si by reactive RF co-sputtering. *Physica Status Solidi (B)*, *235*(1), 111–114. http://doi.org/10.1002/pssb.200301537.

Olesinski, R. W., & Abbaschian, G. J. (1985). The Sb-Si (Antimony-Silicon) system. *Bulletin of Alloy Phase Diagrams*, *6*(5), 445–448. http://doi.org/10.1007/BF02869508.

Prayogi, S., Ayunis, A., Cahyono, Y., & Darminto, D. (2023). N-type H2-doped amorphous silicon layer for solar-cell application, *Mater Renew Sustain Energy*. http://doi.org/10.1007/s40243-023-00232-9.

Ruan, T., Qu, M., Wang, J., He, Y., Xu, X., Yu, C., . . . , & Yan, H. (2019). Effect of deposition temperature of a-Si: H layer on the performance of silicon heterojunction solar cell. *Journal of Materials Science: Materials in Electronics*, *30*(14), 13330–13335. http://doi.org/10.1007/s10854-019-01700-7.

Safi, I. (2000). Recent aspects concerning DC reactive magnetron sputtering of thin films: A review. *Surface and Coatings Technology*, *127*(2–3), 203–218. http://doi.org/10.1016/S0257-8972(00)00566-1.

Schmidt, J. A., Budini, N., Rinaldi, P., Arce, R. D., & Buitrago, R. H. (2009). Nickel-induced crystallization of amorphous silicon. *Journal of Physics: Conference Series*, *167*, 012046. http://doi.org/10.1088/1742-6596/167/1/012046.

Sharma, N., Hooda, M., & Sharma, S. K. (2014). Synthesis and characterization of LPCVD polysilicon and silicon nitride thin films for MEMS applications. *Journal of Materials*, *2014*, 1–8. http://doi.org/10.1155/2014/954618.

Shekoofa, O., Wang, J., Li, D., Luo, Y., Sun, C., Hao, Z., . . . , & Li, H. (2017). P-silicon thin film fabricated by magnetron sputtering and aluminium induced crystallization for Schottky silicon solar cells. *Materials Science in Semiconductor Processing*, *71*, 366–373. http://doi.org/10.1016/j.mssp.2017.06.008.

Shekoofa, O., Wang, J., Li, D., & Luo, Y. (2020). Investigation of microcrystalline silicon thin film fabricated by magnetron sputtering and copper-induced crystallization for photovoltaic applications. *Applied Sciences*, *10*(18), 6320. http://doi.org/10.3390/app10186320.

Tüzün, Ö., Qiu, Y., Slaoui, A., Gordon, I., Maurice, C., Venkatachalam, S., . . . , & Poortmans, J. (2010). Properties of n-type polycrystalline silicon solar cells formed by aluminium induced crystallization and CVD thickening. *Solar Energy Materials and Solar Cells*, *94*(11), 1869–1874. http://doi.org/10.1016/j.solmat.2010.06.031.

Wang, Y., Li, H. Z., Li, D. L., Xing, G. J., Yu, C. N., Gordon, I., & Van Der Biest, O. (2008). Influence of annealing time on crystallization of amorphous SI by SB, *Synthesis and Reactivity in Inorganic, Metal-Organic, and Nano-Metal Chemistry*, *38*(3), 297–302. http://doi.org/10.1080/15533170802023494.

Wilken, K., Güneş, M., Wang, S., Finger, F., & Smirnov, V. (2022). Understanding the origin of thermal annealing effects in low-temperature amorphous silicon films and solar cells. *Physica Status Solidi (a)*, *219*(9), 2100451. http://doi.org/https://doi.org/10.1002/pssa.202100451.

**How to Cite:** Shekoofa, O., Wang, J., & Li, D. (2024). Fabrication of N-Type Nanocrystalline Silicon Thin Film by Magnetron Sputtering and Antimony-Induced Crystallization. *Archives of Advanced Engineering Science*, *2*(2), 71–78. https://doi.org/10.47852/bonviewAAES32021040